Characterizing the Cooperativity in H-Bonded Amino Structures†

Tanja van Mourik*,#,§ and Andrew J. Dingley‡,£

Chemistry Department, University College London, 20 Gordon Street, London WC1H 0AJ, U.K., School of Chemistry, University of St. Andrews, North Haugh, St. Andrews, Fife, KY16 9ST, Scotland, U.K., Department of Biochemistry and Molecular Biology, University College London, Gower Street, London WC1E 6BT, U.K., and Department of Chemistry, The University of Auckland, Auckland, New Zealand

Received: March 26, 2007; In Final Form: May 24, 2007

Density functional theory calculations were used to examine the effect of H-bond cooperativity on the magnitude of the NMR chemical shifts and spin−spin coupling constants in a C_{4h}-symmetric G-quartet and in structures consisting of six cyanamide monomers. These included two ring structures (a planar C_{6h}-symmetric structure and a nonplanar S_6-symmetric structure) and two linear chain structures (a fully optimized planar C_s-symmetric chain and a planar chain structure where all intra- and intermolecular parameters were constrained to be identical). The NMR parameters were computed for the G-quartet and cyanamide structures, as well as for shorter fragments derived from these assemblies without reoptimization. In the ring structures and the chain with identical monomers, the intra- and intermolecular geometries of the cyanamides were identical, thereby allowing the study of cooperative effects in the absence of geometry changes. The magnitude of the $|^1J_{NH}|$ coupling, ^{1}H and ^{15}N chemical shifts of the H-bonding amino N−H group, and the $|^{h2}J_{NN}|$ H-bond coupling increased, whereas the size of the $|^1J_{NH}|$ coupling of the non-H-bonded amino N−H bonds of the first amino group in the chain, which are roughly perpendicular to the H-bonding network, decreased in magnitude when H-bonding monomers were progressively added to extending ring or chain structures. These effects are attributed to electron redistribution induced by the presence of the nearby H-bonding guanine or cyanamide molecules.

1. Introduction

Hydrogen bond (H-bond) interactions are often treated using pairwise energy potentials, which do not properly account for the cooperative nature of H-bonding interactions, yet such cooperativity is a key biological process in biomacromolecular folding and stability. Cooperative interactions in H-bonded assemblies are defined as the difference between the total interaction energy of a H-bonding chain of molecules and the sum of the pairwise H-bonding interaction energies. Various molecular properties are influenced by cooperativity effects, including geometric and vibrational properties.[1−3] Theoretical investigations examining H-bond cooperativity in peptides, formamide chains, and chains of HCN and HNC molecules have provided valuable data on cooperativity effects in H-bonded assemblies.[2−8] For example, in formamide chains, the central H-bonds were calculated to be significantly stronger than those located at the ends, and this effect increased as the chain length increased.[5]

The experimental observation of spin−spin coupling constants between nuclei across the H-bond in chemical and biological systems[9−35] provides a direct approach for identifying the presence of H-bonds. These initial discoveries have led to numerous experimental and theoretical studies examining the character of the H-bonds in various chemical and biological molecules.[36] Since spin−spin couplings are exquisitely sensitive to structural changes, H-bond couplings (HBC) provide an ideal probe for exploring H-bond geometric properties and cooperativity in H-bonded systems. Recent density functional theory (DFT) and ab initio molecular orbital methods examining N−H···O═C, N−H···N, N−H···C, and C−H···N moieties have shown correlations between H-bond geometry and HBCs.[37−48] In addition, calculations have investigated H-bond cooperativity effects in which the H-bond geometries are identical between H-bonding moieties yet the size of the HBCs differ throughout the H-bonding chain.[49] Experimental research by Juranić and co-workers[50,51] has shown that HBCs are sensitive to the extended environment of a H-bonded system and have provided correlations between intramolecular and intermolecular spin−spin couplings in a protein backbone context.

DNA quadruplexes form tandem repeats of short guanine-rich sequences found in telomeres and are recognized to play important biological roles, interact with a number of proteins, and pose as potential therapeutic targets against cancer. The guanine quartet (G-quartet) structural motif found in quadruplexes is characterized by four in-plane guanine bases hydrogen bonded together in a cyclic arrangement which is stabilized by the presence of monovalent ions such as K^+ and Na^+. In a recent DFT study, we performed theoretical calculations of NMR parameters related to the (H)N−H···N and N−H···O═C H-bond moieties found in G-quartets and showed that the sizes of the two- ($^{h2}J_{NN}$) and three-bond ($^{h3}J_{NC'}$) HBCs were correlated with various geometric features of the H-bonds.[47] Further DFT investigation of the amino group in cyanamide models and G-quartets revealed that H-bonding and consequent electron redistribution induced by the presence of the H-bond acceptor molecule are responsible for the calculated distance dependen-

† Part of the "Thom H. Dunning, Jr., Festschrift".

University College London and University of St. Andrews.
‡ University College London and University of Auckland.
§ Current address: School of Chemistry, University of St. Andrews, North Haugh, St. Andrews, Fife, KY16 9ST, Scotland, UK. E-mail: tanja.vanmourik@st-andrews.ac.uk.
£ Current address: Department of Chemistry, The University of Auckland, Auckland, New Zealand. E-mail: a.dingley@auckland.ac.nz.

10.1021/jp072379i CCC: $37.00
Published on Web 08/04/2007

cies of one-bond ($^1J_{NH}$) couplings of H-bonded amino groups in G-quartet structures.[52]

There are a number of theoretical investigations that have computed NMR parameters in non-amino N−H···N H-bonds in both chemical and biological contexts.[2−8] In contrast, little information is available on H-bond cooperativity in the biologically important donor amino group. In this article, a C_{4h}-symmetric G-quartet and extended linear and closed-ring H-bonded structures consisting of cyanamide molecules have been studied as models of H-bonded amino group clusters. Quantum chemistry calculations were used to probe the influence of H-bond cooperativity on the magnitude of the NMR chemical shifts and spin−spin coupling constants. The results showed that the size of the $|^1J_{NH}|$ coupling, donor ^{1}H and ^{15}N chemical shifts of the H-bonding amino N−H group, and the $|^{h2}J_{NN}|$ coupling increased, whereas the size of the $|^1J_{NH}|$ coupling of the non-H-bonded amino N−H bonds, which are roughly perpendicular to the H-bonding network, decreased in magnitude as the H-bonding cluster increased in size. These effects are due to electron redistribution induced by the presence of the neighboring H-bonding acceptor guanine or cyanamide molecules.

2. Methodology

2.1. General. All calculations were performed at the density functional theory (DFT) level with the B3LYP functional[53−55] using the Gaussian 03 program package.[56] Gaussian's "ultrafine" integration grid was employed throughout. For consistency with our previous study investigating the NMR parameters in G-quartets,[47] the 6-311G(d) basis set was used for the calculation of the NMR spin−spin couplings and isotropic chemical shifts. This basis set was shown to give reasonable agreement as compared to a larger basis set with decontracted *s* functions.[52] To test the adequacy of the 6-311G(d) basis set for the current research, we recomputed the coupling constants of the C_{6h}-symmetric cyanamide ring (see below) with the aug-cc-pVDZ-su2 basis set (Dunning's aug-cc-pVDZ basis set[57,58] with fully decontracted *s* functions and two additional tight *s* functions, each with an exponent five times larger than the previous one[59]). The aug-cc-pVDZ-su2 basis set contains both diffuse functions, which are necessary for a proper description of intermolecular interactions, and a large number of decontracted *s* functions, which are essential for a proper description of the coupling constants.[59] The calculations showed that the 6-311G(d) basis set used in this work is satisfactory for predicting the cooperativity trends of the coupling constants (see below). The spin−spin coupling constants were calculated as the sum of all four Ramsay terms (i.e., Fermi contact, spin−dipolar, paramagnetic spin−orbit, and diamagnetic spin−orbit)[60] using ^{1}H, ^{13}C, and ^{15}N isotopes. The Fermi contact term dominated the total spin−spin coupling in all cases (Tables S2 and S3 in the Supporting Information). The shielding tensors were computed using the gauge-independent atomic orbital (GIAO) method.[61,62] The isotropic ^{1}H, ^{13}C, and ^{15}N chemical shifts were indirectly referenced to tetramethylsilane (TMS), CH_4, and liquid ammonia, respectively. The TMS (^{1}H) magnetic shielding (32.1 ppm) was obtained from the calculated shielding of gas-phase CH_4 and the experimental difference (0.13 ppm) between gas-phase CH_4 and TMS.[63] The ^{13}C magnetic shielding (190.2 ppm) was calculated from gas-phase CH_4. The liquid NH_3 (^{15}N) magnetic shielding (252.9 ppm) was obtained from the calculated shielding of gas-phase NH_3 and the experimental difference between gas-phase NH_3 and liquid CH_3NO_2 (399.3 ppm),[64,65] and between liquid NH_3 and liquid CH_3NO_2 (381.9 ppm).[66] The gas-phase CH_4 and NH_3 structures were obtained from B3LYP/6-311++G(d,p) geometry optimizations.

The calculations were performed on a cluster of 900 MHz Sunfire V880 servers at the HiPerSPACE Computing Centre at University College London, clusters of 1.7 to 2.8 GHz Pentium 4 and dual processor Xeon PCs, and a cluster of dual-core dual-processor AMD Opteron compute nodes, which is part of the EaStCHEM Research Computing Facility.

2.2. Structure Optimization. NMR chemical shifts and spin−spin coupling constants were computed for a guanine (G) quartet structure and for ring and extended-chain structures consisting of six cyanamide molecules. Cyanamide was used as a model system for guanine as this is the simplest molecule to provide both a donor amino group and acceptor nitrogen atom. Even though the cyano group is a weaker H-bond acceptor compared to the acceptor N7 atom in guanine, we have shown[52] that such a system yields correct trends for distance dependencies of the coupling constants and follows spin−spin coupling profiles previously presented for much stronger H-bond acceptor atoms.[19,39,67,68] In addition, unlike guanine bases, cyanamide molecules can form both ring and extended-chain structures. The structure of the C_{4h}-symmetric G-quartet (Figure 1), optimized at the B3LYP/6-311++G(d,p) level of theory, was taken from previous work.[47] The structure of a ring consisting of six cyanamide molecules was optimized starting from either a C_s- or C_1-symmetric structure using the 6-311++G(d,p) basis set. The C_s-symmetric structure optimized to a ring arrangement of C_{6h} symmetry, whereas the C_1-symmetric structure optimized to a ring of S_6 symmetry (Figure 4). The S_6 ring was found to be a true minimum on the potential energy surface, as evidenced by the absence of imaginary frequencies, whereas nine imaginary frequencies were observed for the C_{6h} ring structure. In addition, linear chain structures consisting of six cyanamide molecules were optimized. The C_1-symmetric cyanamide chain structure was found not to be stable and converged toward a ring structure during optimization. Full optimization within C_s symmetry led to a planar cyanamide chain possessing 11 imaginary frequencies (Figure 4). In contrast to the ring structures, in the C_s-symmetric chain, the geometries of the individual cyanamide monomers are dependent on the position in the chain. To provide a chain structure with identical cyanamide geometries, the planar C_s-symmetric chain structure was also optimized with constraints to ensure all intra- and intermolecular geometries remained identical.

3. Results and Discussion

3.1. Guanine Quartet. Figure 1b,c shows the change in the $^1J_{N2H2}$ and $^{h2}J_{N2N7}$ coupling constants as the number of guanine bases comprising the structure increases from a monomer to a quartet (Figure 1a). The solid lines in Figure 1b,c correspond to the couplings of the first guanine molecule in the structure, whereas the dashed lines correspond to the couplings of the last guanine molecule (Figure 1a). In the monomer and quartet, the distinction between the first and last amino groups is lost, and the solid and dashed lines of the $^1J_{N2H21}$ or $^1J_{N2H22}$ couplings therefore coincide at these points in Figure 1b.

The $|^1J_{N2H21}|$ couplings of the first (solid black line) and last (dashed black line) guanine increased as the number of guanine bases increased, showing a positive cooperativity for this coupling. Similarly, the $|^{h2}J_{N2N7}|$ couplings (Figure 1c) also increased from dimer → trimer → G-quartet. In contrast, the $|^1J_{N2H22}|$ couplings (gray lines in Figure 1b) were computed to be smaller in the G-quartet than those in the monomer. The $|^1J_{N2H22}|$ coupling of the first guanine decreased from monomer

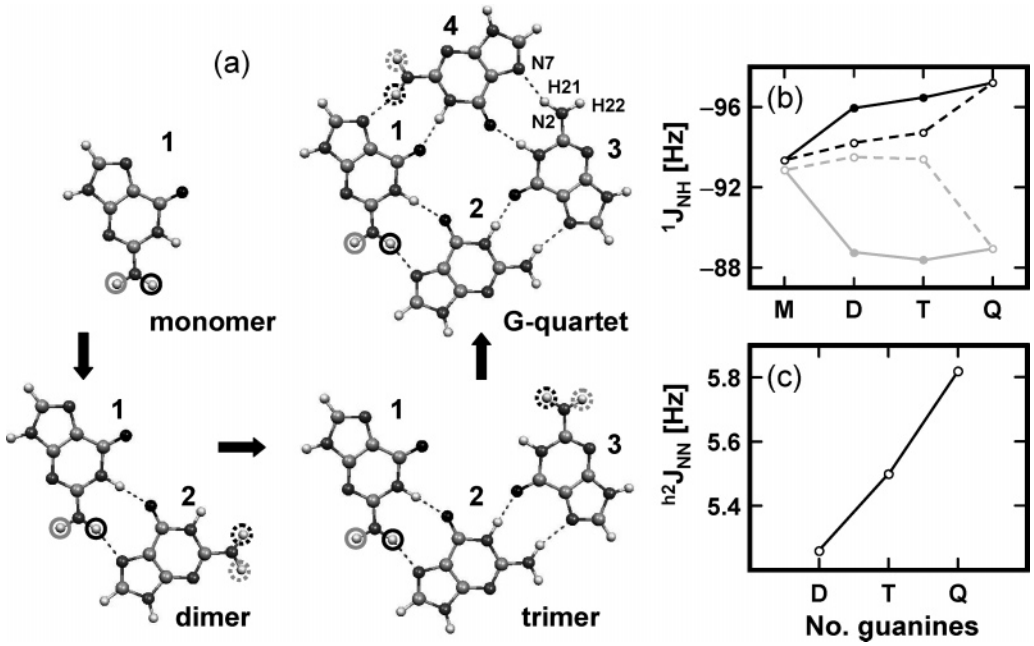

Figure 1. (a) The guanine monomer, dimer, trimer, and G-quartet structures used in this work. All structures are derived without reoptimization from the C_{4h}-symmetric G-quartet structure optimized with B3LYP/6-311++G(d,p). The hydrogen atom H-bonded to the N7 atom (H21) is circled in black, whereas the hydrogen atom (H22) not involved in H-bonding is circled in gray. The solid and dashed circles represent whether the amino group is the first or last in the chain. The monomer (M), dimer (D), trimer (T), and G-quartet (Q) $^1J_{N2H2}$ (b) and $^{h2}J_{N2N7}$ (c) coupling constants are shown. Coupling constants related to the amino group of the first molecule are depicted using solid lines. Coupling constants related to the last molecule are shown with a dashed line and open circles. The black and gray lines refer to the $^1J_{N2H21}$ (H-bonded N−H) and $^1J_{N2H22}$ (free N−H) couplings, respectively.

→ dimer → trimer and then slightly increased going to the quartet, whereas the $|^1J_{N2H22}|$ coupling of the last guanine first slightly increased from monomer to dimer and then decreased from dimer to G-quartet. Thus, the coupling between the N and H atoms of the N2−H21 bonds, which are directly involved in the N2−H21···N7 H-bonding network, increased upon formation of the G-quartet. In contrast, the coupling between the atoms of the N2−H22 bonds, which are roughly perpendicular (i.e., ∠(H22−N2−N7) = 106°) to the N2−H21···N7 H-bond network, decreased upon formation of the G-quartet. As the intra- and intermolecular geometries were identical in all complexes, the changes in the couplings are due to electron redistribution effects caused by the presence of the H-bonding molecules (see below). The opposing trends of $|^1J_{N2H21}|$ and $|^1J_{N2H22}|$ from the guanine monomer to the G-quartet are consistent with the effect of H-bonding on the amino $|^1J_{NH}|$ couplings in formamide−formamide and formamide−formamidine dimers, where the $|^1J_{NH}|$ couplings were found to increase when the coupled proton was engaged in the H-bond and to decrease substantially when the coupling atoms belonged to the free N−H bond.[40] These contrasting trends persisted when monomer relaxation effects were disregarded. Similarly, H-bonding of one or two water molecules to the H22 atom in the guanine monomer was found to increase the $|^1J_{N2H22}|$ and decrease the $|^1J_{N2H21}|$ coupling, even when the guanine geometries were kept identical in the guanine, guanine−$(H_2O)_1$ and guanine−$(H_2O)_2$ molecular systems,[69] further confirming our results that the variation in the couplings is mainly due to electronic and not geometrical effects. The dependence of the $|^1J_{NH}|$ and $|^{h2}J_{N2N7}|$ couplings on the number of guanine molecules in the ring mainly originates from the sensitivity of the FC term (Tables S2 and S3, Supporting Information).

As was also observed for the $|^1J_{N2H22}|$ and $|^{h2}J_{N2N7}|$ couplings, the ^{15}N2 and ^{1}H21 chemical shifts increased as the number of guanine bases constituting the structure increased (Figure 2). The observed ^{1}H21 downfield shift corroborates the observed

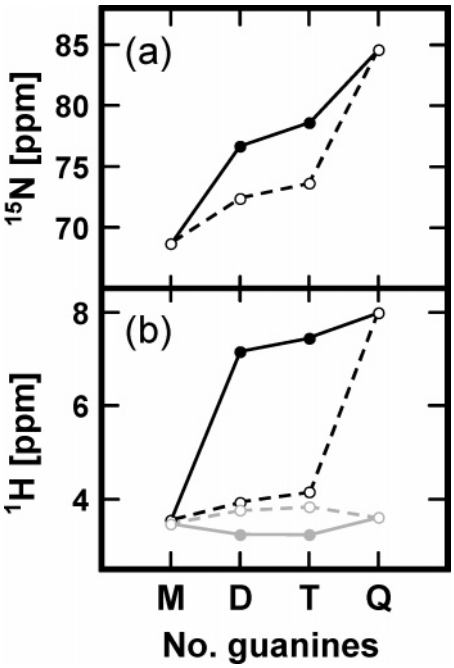

Figure 2. The guanine monomer (M), dimer (D), trimer (T), and G-quartet (Q) ^{15}N2 (a) and ^{1}H2 (b) chemical shifts are shown. Solid lines: coupling constants related to the amino group of the first molecule. Dashed lines: coupling constants related to the last molecule. The black and gray lines refer to the ^{1}H21 and ^{1}H22 couplings, respectively.

trend computed for the $^{h2}J_{N2N7}$ couplings in which the N2−H2···N7 H-bonds strengthen as the H-bonding network increases. Similar large increases (from ∼4 to 6−7 ppm) in the ^{1}H2 chemical shift have also been observed for H-bonding of one or two water molecules to the H22 atom of a guanine molecule.[69] The proton chemical shifts of the H22 atoms, on the other hand, showed significantly smaller changes in

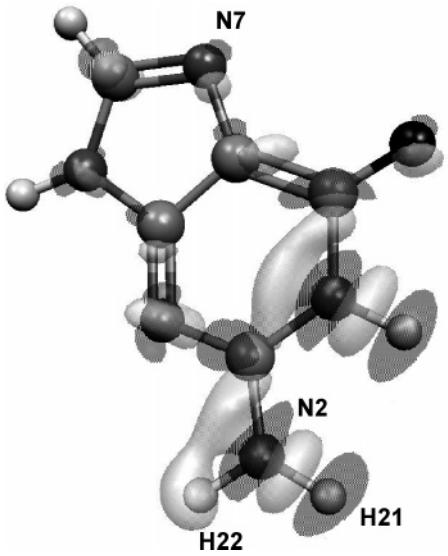

Figure 3. Electron difference density distribution obtained by subtracting the electron density of a guanine monomer from the H-bond donor guanine molecule (with identical geometry as the guanine monomers in the G-quartet) in the dimer structure (derived without reoptimization from the G-quartet structure). The electron densities were computed with B3LYP/6-311++G(d,p). Light-gray areas show an increase in the electron density, whereas dark-gray areas show a decrease in the electron density. The cutoff was set at 0.001 au.

magnitude, but with a similar pattern as that observed for the $|^1J_{N2H22}|$ couplings (Figure 1).

Similar increases in the magnitude of the H-bonding amino $|^1J_{NH}|$ coupling upon H-bonding, with concomitant decreases in the non-H-bonded amino $|^1J_{NH}|$ coupling, have been observed in the cyanamide dimer.[52] This was explained by the charge polarization caused by the electric field of the H-bonding second cyanamide molecule in the dimer (the so-called electric field effect[68,70]). Negative charge is pushed from the H-bonding hydrogen onto the donor amino nitrogen and free hydrogen atom by the negative charge (i.e., electric charge) of the acceptor nitrogen atom, thereby leading to an increase in the H-bonding $|^1J_{NH}|$ and a decrease in the free $|^1J_{NH}|$ coupling. Figure 3 shows the electron difference density distribution obtained by subtracting the electron density of a guanine molecule from that of the H-bond donor guanine molecule in the dimer (derived without reoptimization from the G-quartet structure). The electron difference density distribution shows the change in the electron density of an isolated guanine molecule upon addition of a second guanine molecule (acting as the H-bond acceptor). The electron density at the H-bond-donating side of the N2 atom has increased. The electron density on H21 has decreased, whereas the H22 atom displays an increase in electron density. These results are corroborated by the changes in the natural bond order (NBO) charges[71−73] (Table S5, Supporting Information), which show that N2 is more negative, H21 more positive, and H22 less positive in the guanine dimer as compared to the monomer. Very similar electron difference density distribution patterns were previously observed for the cyanamide dimer,[52] indicating that the electric field effect is also responsible for the coupling trends in the G-quartet. An analogous electron difference density distribution of the N1−H1 bond was also observed (Figure 3). Here, the acceptor O6 atom in the N1−H1···O6 H-bond induces a similar change in the electron distribution of the donor moiety as that of the acceptor N7 atom in the N2−H2···N7 H-bond moiety. Similar to what was observed for $|^1J_{N2H21}|$, the $|^1J_{N1H1}|$ couplings of the donor molecule also increased, whereas the $|^1J_{N1H1}|$ couplings of the acceptor molecule decreased as the number of guanine bases increased (Figure S1 Supporting Information). Similar to the observed trend of the $|^{h2}J_{N2N7}|$ couplings (Figure 1c), the $|^{h3}J_{N1C6}|$ couplings also increased as the number of guanine bases increased (Figure S2, Supporting Information). Accordingly, an increase in the magnitude of the H-bond coupling constants is computed for both H-bond couplings.

There is a close correspondence between the guanine and cyanamide dimer results with respect to the electron difference density and the changes in the magnitude of the $^1J_{NH}$ couplings upon H-bonding. This indicates that cyanamide is a reasonable model for the amino group in guanine structures, even though the cyano group is a much weaker H-bond acceptor[74,75] than the acceptor nitrogen atom in guanine. Thus, in the remainder of this investigation, we have used cyanamide to study the cooperativity of the NMR parameters related to the amino group. The additional advantage of studying cyanamide is that both closed-ring and linear chain structures can be formed, thus providing two different structural motifs to study H-bond cooperativity in amino H-bonding systems.

3.2. Cyanamide Rings and Chains. Figure 4 shows the change in the $|^1J_{NH}|$ couplings for both the H-bonded N−H (i.e., $^1J_{N2H21}$) and non-H-bonded N−H (i.e., $^1J_{N2H22}$) moieties of the cyanamide amino group. The change in the $^1J_{NH}$ couplings is shown as a function of increasing cyanamide molecules in both C_{6h}-symmetric (Figure 4a,e) and S_6-symmetric ring structures (Figure 4b,f). The $|^1J_{NH}|$ couplings as a function of cyanamide number have also been calculated using two different chain structures (Figure 4c,d,g). Due to the symmetry of the ring structures, all individual cyanamide geometries were identical. However, this was not the case for the planar cyanamide chain (Figure 4c,g), where the cyanamide monomers adopt different geometries due to H-bond cooperativity (i.e., a contraction of the H-bonds is observed toward the midpoint of the chain). This chain structure was therefore also optimized with constraints to keep all corresponding intra- and intermolecular geometric values identical (Figure 4d).

In general, the $|^1J_{N2H21}|$ couplings increased with growing chain length for both ring and chain structures. Two exceptions to this general trend were observed: (i) the closure of the ring structure by the addition of the sixth cyanamide molecule in the C_{6h}-symmetric ring led to a decrease in the $|^1J_{N2H21}|$ coupling magnitude (Figure 4a, dashed black line); and (ii) the coupling of the last cyanamide in the C_s-symmetric chain decreased in magnitude for chain lengths beyond the trimer (Figure 4c, dashed black line). Besides the C_{6h}-symmetric cyanamide ring, the $|^1J_{N2H21}|$ couplings of the first cyanamide molecule (solid black line) were computed to be larger than the $|^1J_{N2H21}|$ couplings of the last cyanamide molecule (dashed black line). The smaller magnitude of the $|^1J_{N2H21}|$ couplings of the first cyanamide molecule compared to that of the last molecule in the C_{6h} ring structure is related to the shorter R_{NN} distance in this structure (2.88 as compared to 2.94 Å in the planar chain with identical cyanamide geometries); increasing R_{NN} in the dimer fragment obtained from the C_{6h}-symmetric ring structure decreased the $|^1J_{N2H21}|$ coupling of the first molecule to a smaller extent than that of the last molecule, with the result that the $|^1J_{N2H21}|$ coupling of the first molecule was larger than that of the last molecule for R_{NN} distances $> \sim 2.9$ Å (data not shown). The larger magnitude of the $|^1J_{N2H21}|$ coupling as compared to the $|^1J_{N2H22}|$ coupling of the last molecule in the fully optimized planar chain (dashed lines in Figure 4c) is related to the differences in the corresponding R_{N2H2} distances (see inset, Figure 4c). The R_{N2H21} distance in the fully optimized planar

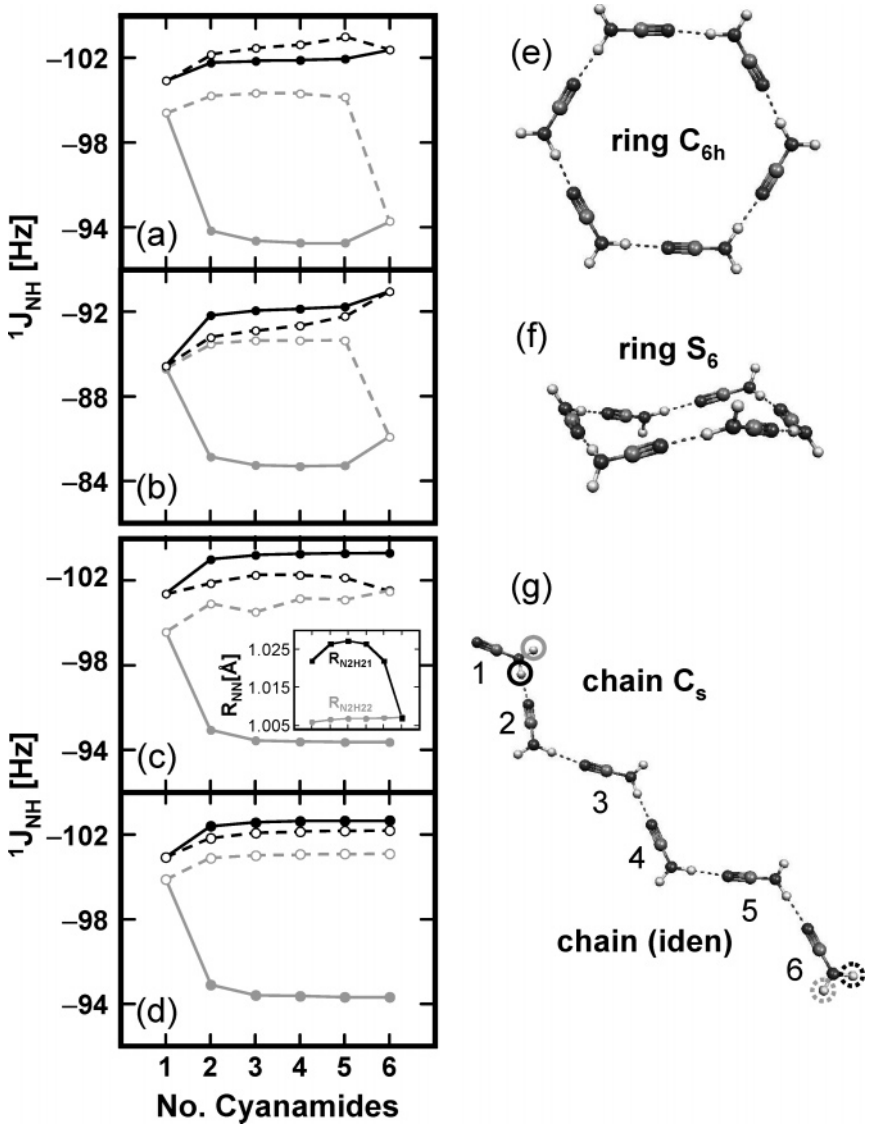

Figure 4. $^1J_{NH}$ coupling constants in the planar C_{6h}-symmetric cyanamide ring structure (a), the S_6-symmetric ring structure (b), the fully optimized (within symmetry restrictions) planar C_s-symmetric chain structure (c), and the planar C_s-symmetric chain structure with identical cyanamide geometries (d). Solid lines: coupling constants related to the amino group of the first molecule. Dashed lines: coupling constants related to the last molecule. The black and gray lines refer to the $^1J_{N2H21}$ and $^1J_{N2H22}$ couplings, respectively. The C_{6h} ring, S_6 ring, and C_s chain structures are shown in (e), (f), and (g), respectively. Only the fully optimized C_s chain structure is shown since the two chain structures are indistinguishable on the scale of the figure. Inset, Figure 4c: R_{N2N21} and R_{N2H22} distances as a function of the monomer position in the chain.

chain was largest toward the middle of the chain due to H-bond cooperativity. The larger R_{N2H21} values compared to the R_{N2H22} distances led to larger $|^1J_{N2H21}|$ couplings. This is in agreement with our previous results which showed that the size of the (non-H-bonded) amino $|^1J_{NH}|$ coupling in the cyanamide monomer increased with increasing N−H bond length.[52] In the hexamer, where both N2−H2 bonds of the amino group are not H-bonded in the last molecule, the R_{N2H21} and R_{N2H22} distances were very similar, leading to almost identical coupling values. Figure 4c shows that the trend of the $|^1J_{N2H21}|$ couplings follows that of R_{N2H21}. Provasi et al. studied the cooperative effects in linear HCN and HNC complexes[8] and observed that the effect of the other molecules in a chain leads to an increase in the magnitude of a given intramolecular spin−spin coupling. The only exception in this study is the $^1J_{NH}$ coupling of the H-bond-donating N−H moiety in the linear HNC chain, which decreases in magnitude upon H-bonding. Thus, the size of this coupling is largest when it is not involved in a H-bond, which is in contrast to the cooperativity effect on the $^1J_{CH}$ coupling in the linear HCN complexes and also in contrast to the variation of the $^1J_{NH}$ coupling in the cyanamide chains presented in this paper.

The $|^1J_{N2H22}|$ coupling of the first monomer (solid gray lines) generally decreased with increasing chain length (except upon ring closure). The largest decrease (∼5 Hz) was computed upon progressing from the monomer to the dimer structure in all models studied. Similarly, in the ring structures, the $|^1J_{N2H22}|$ couplings of the last monomer (dashed gray lines) showed a large decrease in magnitude upon ring closure. The large decreases from the monomer to the dimer (coupling of first cyanamide) and from the pentamer to the hexamer (coupling of last cyanamide) are related; both are caused by the addition of a H-bonding acceptor cyanamide molecule to the corresponding donor amino group. From the monomer to the dimer structure, a cyanamide molecule was added to the amino group of the first molecule, leading to a large decrease in the $|^1J_{N2H22}|$ coupling of the first cyanamide, whereas moving from the pentamer to the hexamer structure led to ring closure, with the result that the previously non-H-bonded amino group of the last

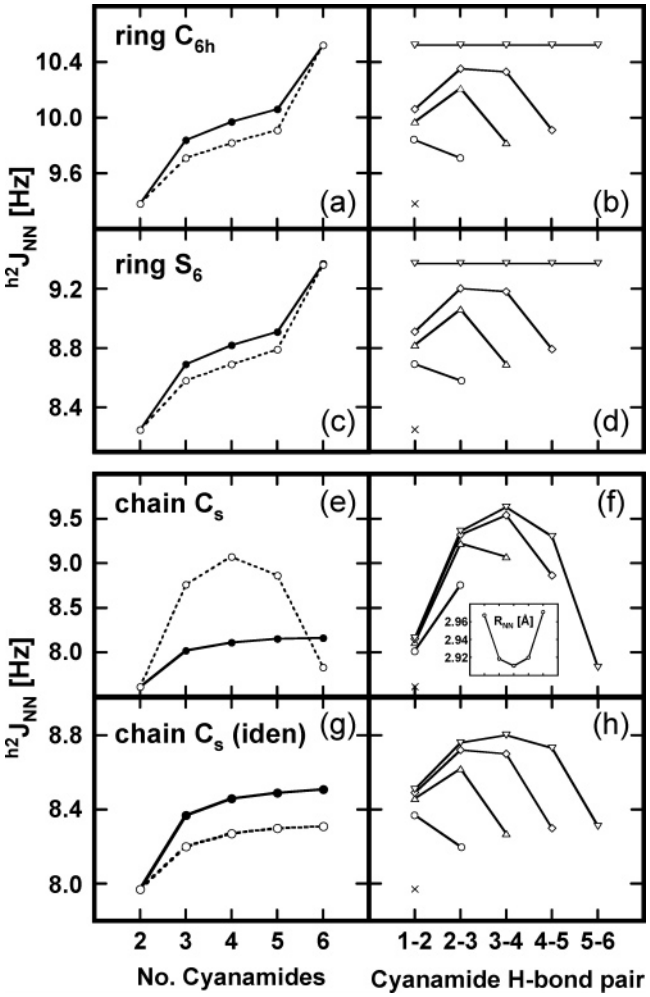

Figure 5. $^{h2}J_{NN}$ coupling constants in the C_{6h} cyanamide ring structure (a,b), the S_6 ring structure (c,d), the fully optimized C_s chain structure (e,f), and the C_s chain structure with identical cyanamide geometries (g,h). In (a), (c), (e), and (g), the solid lines refer to the coupling constants related to the amino group of the first two cyanamide molecules, whereas the dashed lines refer to the coupling constants related to the last two cyanamide molecules. Figures (b), (d), (f), and (h) show the couplings as a function of the sequence position in the different ring or chain fragments. Crosses: cyanamide monomer. Circles: dimer. Triangles: trimer. Squares: tetramer. Inverted triangles: hexamer. Inset, Figure 5f: R_{NN} distance as a function of the monomer position in the C_s chain.

monomer was H-bonded. In the chain structures, the decrease in the $|^1J_{N2H22}|$ coupling of the last monomer did not occur because the amino group of this molecule remained free.

The $|^1J_{NH}|$ couplings are ~10 Hz larger for the planar C_{6h}-symmetric ring compared to the nonplanar S_6-symmetric ring. This difference is due to the increased pyramidality of the amino group in the nonplanar cyanamide monomers in the S_6-symmetric ring. The increased pyramidality gives rise to an increase in the *s* character of the nitrogen lone-pair and a concomitant decrease in the $|^1J_{NH}|$ couplings.[52,76,77]

Figure 5 shows the variation of the $^{h2}J_{NN}$ couplings with increasing ring and chain length. In the ring structures, the $^{h2}J_{NN}$ couplings increased from dimer to hexamer, with the largest changes occurring from dimer to trimer and upon ring closure (Figure 5a,c). In the fully optimized chain structure, the $^{h2}J_{NN}$ couplings of the last cyanamide pair showed a different pattern; the couplings first increased and then decreased upon chain lengthening (dashed line in Figure 5e). This was caused by the decrease in R_{NN} toward the middle of the chain (see inset in Figure 5f), which is a direct effect of H-bond cooperativity. Similar cooperativity-induced contractions of the H-bond distances have also been observed in linear chains of formamide,[5] HCN, and HNC[8] molecules, in α-helices,[2] in *β*-sheet strands consisting of glycine residues,[78] and in chains of *cis*-triaziridine[79] and 4-pyridone residues.[80] It is generally observed that $^{h2}J_{NN}$ couplings decrease exponentially with increasing distance between the coupling atoms,[14,15,19,41,47,49] explaining the inverse relation between R_{NN} and $^{h2}J_{NN}$ in Figure 5f. The exponential dependence of $^{h2}J_{NN}$ on the R_{NN} distance arises from the square of the overlap integrals between the atomic orbitals on the coupling atoms,[41] which decreases exponentially with distance. The very similar shapes of the dashed curve in Figure 5e and the inset in Figure 5f indicate that the magnitude of the $^{h2}J_{NN}$ couplings of the last cyanamide pair was directly related to the R_{NN} distance. In the chain with identical cyanamide monomers (where all R_{NN} were 2.943 Å), the $^{h2}J_{NN}$ couplings did not show the parabola-like trend (Figure 5g), confirming that this trend was primarily due to geometric effects. However, the $^{h2}J_{NN}$ couplings in the chain with identical monomers did not remain constant upon chain lengthening (the $^{h2}J_{NN}$ couplings increased monotonically), which shows that geometric effects are not the only factor that defines the magnitude of the couplings. Clearly, the presence of neighboring (H-bonding) molecules also affects the $^{h2}J_{NN}$ magnitudes even in the absence of geometry variations. Excluding the ring closure effects in the two cyanamide ring structures, the variation of the $^{h2}J_{NN}$ couplings with increasing number of cyanamide molecules was very similar in the ring and chain structures. In the cyanamide chain structure, this trend could only be revealed by keeping the monomers identical.

Figure 5 also shows the $^{h2}J_{NN}$ couplings as a function of the sequence position in the different ring or chain fragments (Figure 5b,d,f,g). The $^{h2}J_{NN}$ couplings were calculated to be strongest for H-bonds located in the middle of the chain. The couplings at the H-bond-donating side were computed to be larger than those at the H-bond acceptor side. Similar trends were also observed for the $^{h2}J_{NC}$ couplings in linear chains of HCN and HNC[8] molecules and in chains of formamides.[49] The changes in the $^{h2}J_{NN}$ couplings were larger in the fully optimized chain structure than those in the chain with identical monomers. This is due to changes in the R_{NN} values throughout the chain. In the closed rings (hexamers), the couplings were identical for all cyanamide pairs due to symmetry. These plots show a remarkable resemblance to those corresponding to the computed H-bond lengths, organized by H-bond position, in formamide chains of different lengths.[5] As all figures except Figure 5f are for structures with identical intermolecular geometries, the increase of $^{h2}J_{NN}$ toward the middle of the ring and upon ring/chain lengthening cannot be due to chain contraction, suggesting that even without the chain contraction, the H-bonds in the center of the chain have increased strength. Presumably, the variation of both R_{NN} and $^{h2}J_{NN}$ follows from electron redistribution caused by H-bond cooperative effects.

To test the adequacy of the 6-311G(d) basis set for calculating the variation in the coupling constants with increasing cyanamide molecules, we recomputed the couplings of the C_{6h}-symmetric cyanamide ring structure (Figures 4a and 5a,b) using the aug-cc-pVDZ-su2 basis set, which contains fully decontracted *s* functions as well as two additional tight *s* functions. Although the absolute values of the couplings computed with aug-cc-pVDZ-su2 were slightly larger than those computed with 6-311G(d), the variation of the couplings with increasing cyanamide molecules was basically identical when calculated with 6-311G(d) and aug-cc-pVDZ-su2 (Figures S3 and S4,

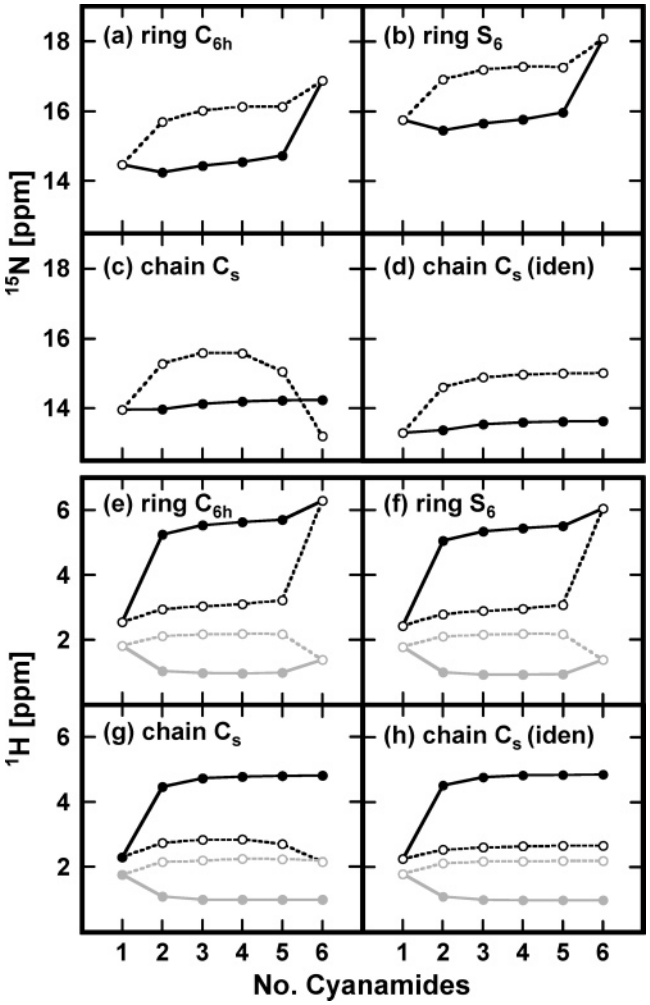

Figure 6. ^{15}N2 (left side, a−d) and ^{1}H2 (right side, b−h) chemical shifts in the C_{6h} cyanamide ring structure (a,e), the S_6 ring structure (b,f), the fully optimized C_s chain structure (c,g), and the C_s chain structure with identical cyanamide geometries (d,h). Solid lines: chemical shifts related to the amino group of the first molecule. Dashed lines: chemical shifts related to the last molecule. The black and gray lines refer to the ^{1}H21 and ^{1}H22 values, respectively.

Supporting Information), indicating that the 6-311G(d) basis set used in this work is satisfactory for predicting the cooperativity trends of the coupling constants.

Figure 6 shows the changes in the ^{15}N2, ^{1}H21, and ^{1}H22 chemical shifts upon ring and chain lengthening. The ^{15}N2 chemical shifts are much smaller (∼13−18 ppm) as compared to the corresponding values in the G-quartet (∼68−85 ppm). In contrast to the G-quartet results (Figure 2), the chemical shifts of the first molecule are smaller than those of the last molecule. The ^{15}N values of the first molecule (solid lines) change slightly with increasing ring and chain size. In the ring structures, the only significant increase in this property occurs upon ring closure. The ^{15}N chemical shifts of the last molecule (dashed lines) show the largest increase from monomer to dimer and upon ring closure in the ring structures. The parabola-shaped curve of the ^{15}N chemical shift of the last molecule in the fully optimized planar chain (Figure 6c) is related to the H-bond contraction toward the middle of the chain, with concomitant increase in R_{N2H21} (inset, Figure 4c). In the chain fragments of increasing length, the last molecule corresponds to the next cyanamide monomer in the chain.

Although ∼2 ppm smaller in magnitude than the ^{1}H chemical shifts of the G-quartet, the ^{1}H values of the cyanamide rings (Figure 6e,f) showed patterns similar to those observed for the G-quartet (Figure 2); the ^{1}H21 values (black lines) increased with increasing ring and chain length. The largest increases occurred from monomer to dimer for ^{1}H21 of the first molecule (solid lines) and, upon ring closure, for ^{1}H21 of the last molecule (dashed lines). The changes in ^{1}H22 (gray lines) are much smaller, as was also observed for the G-quartet. In the cyanamide chains (Figure 6g,h), the ^{1}H21 values also increased with increasing chain length. The largest change occurred from monomer to dimer; from dimer onward, there was minimal change in the magnitude of the chemical shifts. In the fully optimized planar chain (Figure 6g), the ^{1}H21 values of the last molecule decreased from tetramer to hexamer. This is again related to the monomer geometry changes throughout the chain caused by H-bond cooperative effects; the R_{N2H21} distance increased from 1.022 (first monomer) to 1.027 (third monomer) and then decreased again to 1.022 Å (fifth monomer). The smallest value of R_{N2H21} (1.007 Å) was found in the sixth monomer, where the amino group was not H-bonded. Figure 6h shows that this decrease in the magnitude of ^{1}H21 was not computed when the R_{N2H21} distance was identical (1.012 Å) in all cyanamide monomers.

4. Summary

Density functional theory calculations were used to investigate the H-bond cooperative effects on the magnitude of the chemical shifts and spin−spin coupling constants related to the amino group involved in the N−H(amino)···N H-bonding region in G-quartets and ring and chain structures consisting of six cyanamide molecules. The structures were a C_{4h}-symmetric G-quartet, two cyanamide ring structures (a planar C_{6h}-symmetric structure and a nonplanar S_6-symmetric structure), and two linear cyanamide chain structures (a fully optimized planar C_s-symmetric chain and a planar chain structure where all intra- and intermolecular parameters were constrained to be identical). By computing the NMR parameters in fragments derived, without reoptimization, from the G-quartet and cyanamide hexamers, the effect of the addition of H-bonding monomers to incomplete rings and chains was examined.

The magnitude of NMR chemical shifts and spin−spin coupling constants is, in general, dependent upon the electronic structure of the molecule of interest. As also the geometry is a consequence of molecular electronic structure, there is often a close relationship between the chemical shift or spin−spin coupling constant and local geometrical factors, with the result that a variation in the magnitude of the NMR parameters can frequently be explained using geometric considerations. For example, in the fully optimized planar chain of cyanamide molecules, H-bond cooperative effects resulted in a contraction of the H-bonds toward the middle of the chain; the N···N and H···N distances decreased, and the H-bonding amino N−H distance increased toward the chain center. These geometry changes were accompanied by increases in both $|^{1}J_{NH}|$ and $|^{h2}J_{NN}|$ for N−H and N···N bonds located in the center of the chain.

In this Article, we show that in the absence of geometric variations, the magnitude of the NMR parameters change when H-bonding monomers are progressively added to extending ring or chain structures. This was shown for the G-quartet, the cyanamide rings, and the linear cyanamide chain with identical monomers. Due to the presence of symmetry in the G-quartet and cyanamide ring structures and due to optimization constraints in the linear cyanamide chain with identical monomers, all fragments derived from these structures have identical intra-

and intermolecular geometries. Therefore, the computed differences in the NMR parameters in various fragments obtained from the same structure are entirely due to electron redistribution effects caused by adjacent H-bonding guanine or cyanamide molecules. The results showed that, in general, the magnitude of the NMR properties along the H-bond network (i.e., the $|^1J_{NH}|$ coupling and ^1H and ^{15}N chemical shifts of the H-bonding amino N−H group, and the $|^{h2}J_{NN}|$ *trans*-H-bond coupling) increased in magnitude ("positive cooperativity") for structures containing a larger number of monomers. In contrast, the magnitude of the $|^1J_{NH}|$ coupling of the non-H-bonded amino N−H bonds of the first amino group in the chain, which are roughly perpendicular to the H-bonding network, decreased in magnitude ("negative cooperativity") for structures containing a larger number of monomers. The electron difference density obtained by subtracting the electron density of the H-bond-accepting guanine molecule from that of a guanine dimer corroborates the opposite cooperativity effects for the H-bonding and free N−H bonds; the charge density on the hydrogen of the free N−H bond had increased, whereas the H-bonding hydrogen showed a decrease in electron density.

Excluding the ring closure effects in the two cyanamide ring structures, very similar trends were observed for the NMR properties in the G-quartets, cyanamide ring structures, and the linear chain with identical monomers, indicating that similar H-bond cooperative effects operate in rings and chains. These trends were not always evident for the fully optimized planar cyanamide chain due to the large geometric influences on the magnitude of the NMR parameters.

Acknowledgment. T.v.M. is indebted to Thom Dunning for a scientifically stimulating time at the Pacific Northwest National Laboratory. T.v.M. gratefully acknowledges support from the Royal Society via the University Research Fellowship scheme, support from the Engineering and Physical Sciences Research Council (through Grants GR/R63196/01 and GR/S06233/01), and computational support from EaStCHEM via the EaStCHEM Research Computing Facility. A.J.D. acknowledges support from the University of Auckland staff research fund.

Supporting Information Available: Cartesian coordinates of the B3LYP/6-311++G(d,p) optimized geometries of the G-quartet and the cyanamide ring and chain structures (Table S1A−E); contributions to the $^1J_{N2H21}$ and $^1J_{N2H22}$ coupling constants computed for the G-quartet and the cyanamide ring and chain structures (Table S2A−E); contributions to the $^{h2}J_{NN}$ coupling constants (Table S3A−E); and $^{15}N2$, $^1H21$, and $^1H22$ chemical shifts (Table S4A−E). NBO charges in the guanine monomer and dimer (Table S5). Figures S1 and S2 show the $^1J_{N1H1}$ and $^{h3}J_{N1C6}$ coupling constants in the G-quartet. Figures S3 and S4 show the $^1J_{N2H2}$ and $^{h2}J_{NN}$ coupling constants in the C_{6h}-symmetric cyanamide ring structure, computed with B3LYP/aug-cc-pVDZ-su2. This material is available free of charge via the Internet at http://pubs.acs.org.

References and Notes

(1) Sauer, S. P. A.; Špirko, V.; Paidarova, I.; Kraemer, W. P. *Chem. Phys.* **1997**, *214*, 91.
(2) Wieczorek, R.; Dannenberg, J. J. *J. Am. Chem. Soc.* **2003**, *125*, 8124.
(3) Wieczorek, R.; Dannenberg, J. J. *J. Am. Chem. Soc.* **2003**, *125*, 14065.
(4) Kobko, N.; Paraskevas, L.; del Rio, E.; Dannenberg, J. J. *J. Am. Chem. Soc.* **2001**, *123*, 4348.
(5) Kobko, N.; Dannenberg, J. J. *J. Phys. Chem. A* **2003**, *107*, 10389.
(6) Kobko, N.; Dannenberg, J. J. *J. Phys. Chem. A* **2003**, *107*, 6688.
(7) Wieczorek, R.; Dannenberg, J. J. *J. Am. Chem. Soc.* **2004**, *126*, 14198.
(8) Provasi, P. F.; Aucar, G. A.; Sanchez, M.; Alkorta, I.; Elguero, J.; Sauer, S. P. A. *J. Phys. Chem. A* **2005**, *109*, 6555.
(9) Dingley, A. J.; Grzesiek, S. *J. Am. Chem. Soc.* **1998**, *120*, 8293.
(10) Pervushin, K.; Ono, A.; Fernandez, C.; Szyperski, T.; Kainosho, M.; Wuthrich, K. *Proc. Natl. Acad. Sci. U.S.A.* **1998**, *95*, 14147.
(11) Cordier, F.; Grzesiek, S. *J. Am. Chem. Soc.* **1999**, *121*, 1601.
(12) Cordier, F.; Rogowski, M.; Grzesiek, S. *J. Magn. Reson.* **1999**, *140*, 510.
(13) Cornilescu, G.; Hu, J.-S.; Bax, A. *J. Am. Chem. Soc.* **1999**, *121*, 2949.
(14) Cornilescu, G.; Ramirez, B. E.; Frank, M. K.; Clore, G. M.; Gronenbaum, A. M.; Bax, A. *J. Am. Chem. Soc.* **1999**, *121*, 6275.
(15) Dingley, A. J.; Masse, J. E.; Peterson, R. D.; Barfield, M.; Feigon, J.; Grzesiek, S. *J. Am. Chem. Soc.* **1999**, *121*, 6019.
(16) Majumdar, A.; Kettani, A.; Skripkin, E. *J. Biomol. NMR* **1999**, *14*, 67.
(17) Majumdar, A.; Kettani, A.; Skripkin, E.; Patel, D. J. *J. Biomol. NMR* **1999**, *15*, 207.
(18) Wöhnert, J.; Dingley, A. J.; Stoldt, M.; Gorlach, M.; Grzesiek, S. *Nucleic Acids Res.* **1999**, *27*, 3104.
(19) Benedict, H.; Shenderovich, I. G.; Malkina, O. L.; Malkin, V. G.; Denisov, G. S.; Golubev, N. S.; Limbach, H.-H. *J. Am. Chem. Soc.* **2000**, *122*, 1979.
(20) Liu, A. Z.; Majumdar, A.; Hu, W. D.; Kettani, A.; Skripkin, E.; Patel, D. D. *J. Am. Chem. Soc.* **2000**, *122*, 3206.
(21) Löhr, F.; Mayhew, S. G.; Rüterjans, H. *J. Am. Chem. Soc.* **2000**, *122*, 9289.
(22) Luy, B.; Marino, J. P. *J. Am. Chem. Soc.* **2000**, *122*, 8095.
(23) Meissner, A.; Sorensen, O. W. *J. Magn. Reson.* **2000**, *143*, 431.
(24) Meissner, A.; Sorensen, O. W. *J. Magn. Reson.* **2000**, *143*, 387.
(25) Mishima, M.; Hatanaka, M.; Yokoyama, S.; Ikegami, T.; Wälchli, M.; Ito, Y.; Shirakawa, M. *J. Am. Chem. Soc.* **2000**, *122*, 5883.
(26) Pervushin, K.; Fernandez, C.; Riek, R.; Ono, A.; Kainosho, M.; Wuthrich, K. *J. Biomol. NMR* **2000**, *16*, 39.
(27) Majumdar, A.; Kettani, A.; Skripkin, E.; Patel, D. J. *J. Biomol. NMR* **2001**, *19*, 103.
(28) Pietrzak, M.; Limbach, H.-H.; Pérez-Torralba, M.; Sanz, D.; Claramunt, R. M.; Elguero, J. *Magn. Reson. Chem.* **2001**, *39*, S100.
(29) Luy, B.; Richter, U.; DeJong, E. S.; Sorensen, O. W.; Marino, J. P. *J. Biomol. NMR* **2002**, *24*, 133.
(30) Cordier, F.; Barfield, M.; Grzesiek, S. *J. Am. Chem. Soc.* **2003**, *125*, 15750.
(31) Giedroc, D. P.; Cornish, P. V.; Hennig, M. *J. Am. Chem. Soc.* **2003**, *125*, 4676.
(32) Shenderovich, I. G.; Tolstoy, P. M.; Golubev, N. S.; Smirnov, S. N.; Denisov, G. S.; Limbach, H.-H. *J. Am. Chem. Soc.* **2003**, *125*, 11710.
(33) Bouvignies, G.; Bernado, P.; Meier, S.; Cho, K.; Grzesiek, S.; Bruschweiler, R.; Blackledge, M. *Proc. Natl. Acad. Sci. U.S.A.* **2005**, *102*, 13885.
(34) Dingley, A. J.; Peterson, R. D.; Grzesiek, S.; Feigon, J. *J. Am. Chem. Soc.* **2005**, *127*, 14466.
(35) Meier, S.; Strohmeier, M.; Blackledge, M.; Grzesiek, S. *J. Am. Chem. Soc.* **2007**, *129*, 754.
(36) Grzesiek, S.; Cordier, F.; Jaravine, V.; Barfield, M. *Prog. Nucl. Magn. Reson. Spectrosc.* **2004**, *34*, 275.
(37) Bagno, A. *Chem.—Eur. J.* **2000**, *6*, 2925.
(38) Bagno, A.; Gerard, S.; Kevelam, J.; Menna, E.; Scorrano, G. *Chem.—Eur. J.* **2000**, *6*, 2915.
(39) Del Bene, J. E. *J. Am. Chem. Soc.* **2000**, *122*, 3560.
(40) Pecul, M.; Leszczynski, J.; Sadlej, J. *J. Phys. Chem. A* **2000**, *104*, 8105.
(41) Barfield, M.; Dingley, A. J.; Feigon, J.; Grzesiek, S. *J. Am. Chem. Soc.* **2001**, *123*, 4014.
(42) Del Bene, J. E.; Perera, S. A.; Bartlett, R. J. *Magn. Reson. Chem.* **2001**, *39*, S109.
(43) Barfield, M. *J. Am. Chem. Soc.* **2002**, *124*, 4158.
(44) Munzarova, M. L.; Sklenar, V. *J. Am. Chem. Soc.* **2002**, *124*, 10666.
(45) Markwick, P. R. L.; Sprangers, R.; Sattler, M. *J. Am. Chem. Soc.* **2003**, *125*, 644.
(46) Munzarova, M. L.; Sklenar, V. *J. Am. Chem. Soc.* **2003**, *125*, 3649.
(47) van Mourik, T.; Dingley, A. J. *Chem.—Eur. J.* **2005**, *11*, 6064.
(48) Del Bene, J. E.; Elguero, J. *J. Phys. Chem. A* **2006**, *110*, 7496.
(49) Salvador, P.; Kobko, N.; Wieczorek, R.; Dannenberg, J. J. *J. Am. Chem. Soc.* **2004**, *126*, 14190.
(50) Juranić, N.; Slobodan, M. *J. Am. Chem. Soc.* **2001**, *123*, 4099.
(51) Juranić, N.; Moncrieffe, M. C.; Likić, V. A.; Prendergast, F. G.; Macura, S. *J. Am. Chem. Soc.* **2002**, *124*, 14221.
(52) van Mourik, T.; Dingley, A. J. *ChemPhysChem* **2007**, *8*, 288.
(53) Becke, A. D. *Phys. Rev. A* **1988**, *38*, 3098.
(54) Lee, C.; Yang, W.; Parr, R. G. *Phys. Rev. B* **1988**, *37*, 785.
(55) Becke, A. D. *J. Chem. Phys.* **1993**, *98*, 5648.

(56) Frisch, M. J.; Trucks, G. W.; Schlegel, H. B.; Scuseria, G. E.; Robb, M. A.; Cheeseman, J. R.; Montgomery, J. A., Jr.; Vreven, T.; Kudin, K. N.; Burant, J. C.; Millam, J. M.; Iyengar, S. S.; Tomasi, J.; Barone, V.; Mennucci, B.; Cossi, M.; Scalmani, G.; Rega, N.; Petersson, G. A.; Nakatsuji, H.; Hada, M.; Ehara, M.; Toyota, K.; Fukuda, R.; Hasegawa, J.; Ishida, M.; Nakajima, T.; Honda, Y.; Kitao, O.; Nakai, H.; Klene, M.; Li, X.; Knox, J. E.; Hratchian, H. P.; Cross, J. B.; Bakken, V.; Adamo, C.; Jaramillo, J.; Gomperts, R.; Stratmann, R. E.; Yazyev, O.; Austin, A. J.; Cammi, R.; Pomelli, C.; Ochterski, J. W.; Ayala, P. Y.; Morokuma, K.; Voth, G. A.; Salvador, P.; Dannenberg, J. J.; Zakrzewski, V. G.; Dapprich, S.; Daniels, A. D.; Strain, M. C.; Farkas, O.; Malick, D. K.; Rabuck, A. D.; Raghavachari, K.; Foresman, J. B.; Ortiz, J. V.; Cui, Q.; Baboul, A. G.; Clifford, S.; Cioslowski, J.; Stefanov, B. B.; Liu, G.; Liashenko, A.; Piskorz, P.; Komaromi, I.; Martin, R. L.; Fox, D. J.; Keith, T.; Al-Laham, M. A.; Peng, C. Y.; Nanayakkara, A.; Challacombe, M.; Gill, P. M. W.; Johnson, B.; Chen, W.; Wong, M. W.; Gonzalez, C.; Pople, J. A. *Gaussian 03*, revision B.04; Gaussian, Inc.: Pittsburgh, PA, 2004.

(57) Dunning, T. H., Jr. *J. Chem. Phys.* **1989**, *90*, 1007.

(58) Kendall, R. A.; Dunning, T. H., Jr.; Harrison, R. J. *J. Chem. Phys.* **1992**, *96*, 6796.

(59) Helgaker, T.; Jaszunski, M.; Ruud, K.; Górska, A. *Theor. Chem. Acc.* **1998**, *99*, 175.

(60) Ramsay, N. F. *Phys. Rev.* **1953**, *91*, 303.

(61) Ditchfield, R. *Mol. Phys.* **1974**, *27*, 789.

(62) Wolinsky, K.; Hilton, J. F.; Pulay, P. *J. Am. Chem. Soc.* **1990**, *112*, 8251.

(63) Kutzelnigg, W.; Fleischer, U.; Schindler, M. *NMR Basic Principles and Progress*; Springer: Berlin, Germany, 1990; p 165.

(64) Litchman, W. M.; Alei, M., Jr.; Florin, A. E. *J. Chem. Phys.* **1969**, *50*, 1031.

(65) Alei, M., Jr.; Florin, A. E.; Litchman, W. M.; O'Brian, J. F. *J. Phys. Chem.* **1971**, *75*, 932.

(66) Witanowski, M.; Stefaniak, L.; Webb, G. A. *Annu. Rep. NMR Spectrosc.* **1993**, *25*, 88.

(67) Del Bene, J. E.; Elguaro, J. *J. Phys. Chem. A* **2004**, *108*, 11762.

(68) Tuttle, T.; Kraka, E.; Wu, A.; Cremer, D. *J. Am. Chem. Soc.* **2004**, *126*, 5093.

(69) van Mourik, T. *J. Chem. Phys.* **2006**, *125*, 191101.

(70) Tuttle, T.; Gräfenstein, J.; Wu, A.; Kraka, E.; Cremer, D. *J. Phys. Chem. B* **2004**, *108*, 1115.

(71) Reed, A. E.; Weinhold, F. *J. Chem. Phys.* **1983**, *78*, 4066.

(72) Carpenter, J. E.; Weinhold, F. *J. Mol. Struct.:THEOCHEM* **1988**, *169*, 41.

(73) Reed, A. E.; Curtiss, L. A.; Weinhold, F. *Chem. Rev.* **1988**, *88*, 899.

(74) Bordwell, F. G.; Drucker, G. E.; Fried, H. E. *J. Org. Chem.* **1981**, *46*, 632.

(75) Bordwell, F. G. *Acc. Chem. Res.* **1988**, *21*, 456.

(76) Ruiz de Azua, M. C.; Giribet, C. G.; Vizioli, C. V.; Contreras, R. H. *J. Mol. Struct.:THEOCHEM* **1998**, *433*, 141.

(77) Contreras, R. H.; Peralta, J. E. *Progress Nucl. Magn. Reson. Spectrosc.* **2000**, *37*, 321.

(78) Viswanathan, R.; Asensio, A.; Dannenberg, J. J. *J. Phys. Chem. A* **2004**, *128*, 92059.

(79) Song, H.-S.; Xiao, H.-M.; Dong, H.-S.; Zhu, W.-H. *J. Phys. Chem. A* **2006**, *110*, 2225.

(80) Chen, Y.-F.; Dannenberg, J. J. *J. Am. Chem. Soc.* **2006**, *128*, 8100.